JVST A
Journal of Vacuum Science & Technology A

Wafer-level uniformity of atomic-layer-deposited niobium nitride thin films for quantum devices

Cite as: J. Vac. Sci. Technol. A **39**, 052401 (2021); https://doi.org/10.1116/6.0001126
Submitted: 07 May 2021 • Accepted: 24 June 2021 • Published Online: 14 July 2021

Emanuel Knehr, Mario Ziegler, Sven Linzen, et al.

COLLECTIONS

Paper published as part of the special topic on Atomic Layer Deposition (ALD)

EP This paper was selected as an Editor's Pick

ARTICLES YOU MAY BE INTERESTED IN

Green CVD—Toward a sustainable philosophy for thin film deposition by chemical vapor deposition
Journal of Vacuum Science & Technology A **39**, 051001 (2021); https://doi.org/10.1116/6.0001125

Effect of O_2 plasma exposure time during atomic layer deposition of amorphous gallium oxide
Journal of Vacuum Science & Technology A **39**, 052408 (2021); https://doi.org/10.1116/6.0001207

Superconducting nanowire single-photon detectors: A perspective on evolution, state-of-the-art, future developments, and applications
Applied Physics Letters **118**, 190502 (2021); https://doi.org/10.1063/5.0045990

© 2021 Author(s).

Journal of Vacuum Science & Technology A

ARTICLE

avs.scitation.org/journal/jva

Wafer-level uniformity of atomic-layer-deposited niobium nitride thin films for quantum devices

Cite as: J. Vac. Sci. Technol. A **39**, 052401 (2021); doi: 10.1116/6.0001126
Submitted: 7 May 2021 · Accepted: 24 June 2021 ·
Published Online: 14 July 2021

View Online

Export Citation

CrossMark

Emanuel Knehr,[1,2,a)] Mario Ziegler,[2] Sven Linzen,[2] Konstantin Ilin,[1] Patrick Schanz,[1] Jonathan Plentz,[2] Marco Diegel,[2] Heidemarie Schmidt,[2,3] Evgeni Il'ichev,[2] and Michael Siegel[1]

AFFILIATIONS

[1]Institute of Micro- and Nanoelectronic Systems, Karlsruhe Institute of Technology (KIT), 76187 Karlsruhe, Germany
[2]Leibniz Institute of Photonic Technology, 07745 Jena, Germany
[3]Institute for Solid State Physics, Friedrich Schiller University Jena, 07743 Jena, Germany

Note: This paper is part of the 2022 Special Topic Collection on Atomic Layer Deposition (ALD).
[a)]**Electronic mail:** emanuel.knehr@kit.edu

ABSTRACT

Superconducting niobium nitride thin films are used for a variety of photon detectors, quantum devices, and superconducting electronics. Most of these applications require highly uniform films, for instance, when moving from single-pixel detectors to arrays with a large active area. Plasma-enhanced atomic layer deposition (ALD) of superconducting niobium nitride is a feasible option to produce high-quality, conformal thin films and has been demonstrated as a film deposition method to fabricate superconducting nanowire single-photon detectors before. Here, we explore the property spread of ALD-NbN across a 6-in. wafer area. Over the equivalent area of a 2-in. wafer, we measure a maximum deviation of 1% in critical temperature and 12% in switching current. Toward larger areas, structural characterizations indicate that changes in the crystal structure seem to be the limiting factor rather than film composition or impurities. The results show that ALD is suited to fabricate NbN thin films as a material for large-area detector arrays and for new detector designs and devices requiring uniform superconducting thin films with precise thickness control.

© 2021 Author(s). All article content, except where otherwise noted, is licensed under a Creative Commons Attribution (CC BY) license (http://creativecommons.org/licenses/by/4.0/). https://doi.org/10.1116/6.0001126

I. INTRODUCTION

Niobium nitride (NbN) thin films are of interest for a variety of superconducting devices, ranging from hot-electron bolometer mixers[1] to microresonators[2] and magnetometers.[3] A first quantum device based on several coherent quantum phase slip (CQPS) junctions has been realized by means of NbN nanowires.[4] The CQPS junctions require ultrathin NbN films acting as strongly disordered superconductors close to the superconductor-insulator transition.[5,6] Extending the area of these films from small chips to wafer-scale is an important requirement for prospective device developments—like a robust quantum current standard based on CQPS—similar to the well-established electronics based on Josephson junctions.

This also applies to superconducting nanowire single-photon detectors (SNSPDs). Single-pixel devices have shown excellent properties for single-photon counting, with high near-infrared detection efficiency,[7] high timing resolution,[8] and low dark-count rates.[9] For emerging applications in imaging[10] and spectroscopy,[11] large arrays of these detectors are required, for which multiple operation concepts have been demonstrated to date.[12–16]

In this transition from few-pixel to kilopixel devices, the uniformity of superconducting thin films over large areas becomes critical in terms of both general feasibility and fabrication yield. In this regard, amorphous thin films like WSi[7,17] and MoSi[18,19] have an advantage over polycrystalline films because of their homogeneous disorder and lack of grain boundaries, which enables patterning with minimal constrictions. Polycrystalline superconductors based on nitrides like NbN,[20] NbTiN,[21] and TaN,[22] on the other hand, enable higher operating temperatures at 4.2 K and exhibit higher switching currents, which lead to a higher signal-to-noise ratio. A sub-3 ps timing jitter[8] and high counting speeds[23] have been demonstrated by detectors made from NbN as well. Nitride-based SNSPDs, however, generally exhibit smaller spectral bandwidths compared to amorphous silicides.[17]

© Author(s) 2021

In an effort to combine the advantages of amorphous and polycrystalline detectors, various changes to the thin film deposition of NbN have been made either by modifications to the established sputtering process[24] or by novel deposition methods like atomic layer deposition (ALD).[6,25,26] Due to the self-limiting growth process, ALD enables a precise thickness control on the monolayer-scale and excellent surface conformity. For the same reason, thin films with high spatial uniformity over large areas are, in principle, easier to achieve by ALD than by epitaxial growth using reactive magnetron sputtering.

The deposition of superconducting ALD-NbN thin films has been optimized[25–27] and SNSPDs made from these films have been shown before.[28] A broadly saturated detection efficiency at 1550 nm wavelength and a high fabrication yield of SNSPDs due to the excellent uniformity of ALD-NbN on the lateral scale of few millimeters have been shown by Cheng *et al.*[29] Recently, Taylor *et al.* have characterized SNSPDs from ALD-NbN up to a wavelength of 2006 nm.[30]

Here, we explore the large-area uniformity of thin ALD-NbN films by investigating the morphological, structural, and superconducting properties spread up to a wafer size of 6 in.

II. EXPERIMENT

A. Sample preparation

NbN films were deposited using an Oxford Instruments *OpAL* ALD system. A nitrogen glovebox around the deposition chamber reduces the concentration of oxygen impurities incorporated during long deposition times.[27] The deposition process consists of alternating steps of the precursor (*tert*-butylimido)-tris (diethylamido)-niobium (TBTDEN) and hydrogen radicals provided by an inductively coupled plasma (ICP) source, with purge steps in between. The precursor provides both niobium and nitrogen atoms, while the hydrogen plasma reacts with the organic compounds (functional groups) of the precursor remaining on the substrate surface. The by-products and residuals are purged in the subsequent step. The substrate holder is heated to 380 °C. A deposition cycle consists of the following steps: TBTDEN (3 s), N_2-purge (7 s), hydrogen plasma (60 s, 8.3 mTorr, 300 W), and N_2-purge (10 s). More details on the deposition process and parameter optimization can be found in Ref. 25.

As substrates, we use (100) silicon with 300 nm thermal oxide. A total of 21 silicon chips of $10 \times 10\,\text{mm}^2$ size were arranged in a cross-like shape with the remote plasma source (75 mm diameter) concentrically placed 23 cm above the center. In the following, the x- and y-coordinates correspond to this position during deposition, $x, y = (0, 0)$ being defined as the center of the substrate table.

Three depositions were conducted: one with a target thickness of 6 nm (130 ALD cycles) for atomic force microscopy (AFM) and electrical measurements, another 6 nm deposition with a 20 nm thick etch-stop Al_2O_3 layer deposited *in situ* prior to NbN for thickness measurements, and one with a thickness of 20 nm (435 ALD cycles) for x-ray diffraction (XRD) and secondary ion mass spectroscopy (SIMS) measurements.

Electrical four-point probe measurements were conducted on microbridges patterned from the NbN films to determine temperature-dependent resistivity and switching current. The NbN bridges are 1 μm wide and 10 μm long (see geometry in the inset of Fig. 3). This comparatively wide structure was chosen to separate film-inherent inhomogeneities from any adverse effect caused by the patterning process. To avoid current crowding and maximize the switching current,[31] the voltage leads to the microbridge are rounded off. The patterns were defined by electron-beam lithography using 130 nm thick ma-N 2401 resist exposed to electrons of acceleration voltage 50 kV with a dose density of 495 $\mu\text{C/cm}^2$. After development, the written structures were transferred into the NbN layer by Ar-ion milling.

The NbN film thickness was measured on steps etched into the samples with the additional Al_2O_3 layer by reactive ion etching (RIE) using CF_4 and oxygen. With an etch rate of 0.5 Å/min compared to 18 nm/min of NbN for etching conditions at hand, the Al_2O_3 layer acts as an etch-stop layer and therefore allows for a well-defined step.

B. Characterization methods

The film thickness and surface roughness were measured using an FRT *MicroProf* tool equipped with an atomic force microscope. The surface was scanned in the non-contact mode with a line speed of 9 μm/s. The film thickness was defined as the mean value of 21 individually measured profiles of the patterned steps on each chip. The surface roughness was taken as the root mean square (RMS) roughness over a scanned area of $5 \times 5\,\mu\text{m}^2$ at various positions.

To analyze the chemical composition of the deposited films, we used a Hiden Analytical *MAXIM SIMS* equipped with a cesium source and with a spot diameter of 20 μm. The 20 nm thick NbN films were sputtered with a rate of 5 nm/s and the composition of the sputtered material was analyzed using a time-of-flight analytical detector. We traced the most relevant elements present in the films: Nb, N, and C. Plateaus in the recorded depth profiles indicate the deposited thin film and were used to extract the intensity of each element. The resulting counts of carbon and nitrogen were normalized with respect to the niobium count at each position to compensate for slight variations of the primary ion current during the measurement. Niobium was chosen as a reference because of two reasons. First, we assume a constant niobium content over the whole area because of the self-limiting ALD process and the saturation of the surface with TBTDEN. In previous studies, we found that the main impact on film composition stems from the plasma step.[6,25] Second, the sputter rate of niobium should be less dependent on the surrounding chemical bonds because of its higher atomic weight as opposed to carbon and nitrogen. Because the ionization probability of each element is different, the curves of N and C were normalized and absolute values cannot be compared between the elements.

We evaluated changes of the crystallinity and lattice parameter across the deposition area using a PANalytical *X'Pert Pro* x-ray diffractometer equipped with a Cu K_α source. Because of the small film thickness, the samples were mainly analyzed in grazing incidence ($\omega = 0.4°$) with a parallel beam setup instead of standard Bragg–Brentano configuration. The scan time in the 2Θ-range (33°–44°) was kept constant at 40 min for each sample.

The superconductivity parameters were measured in a LHe-cooled dipstick using a current source (Keithley *6221*) and a voltmeter (Keithley *2182A*). A total of 68 microbridges (four per

© Author(s) 2021

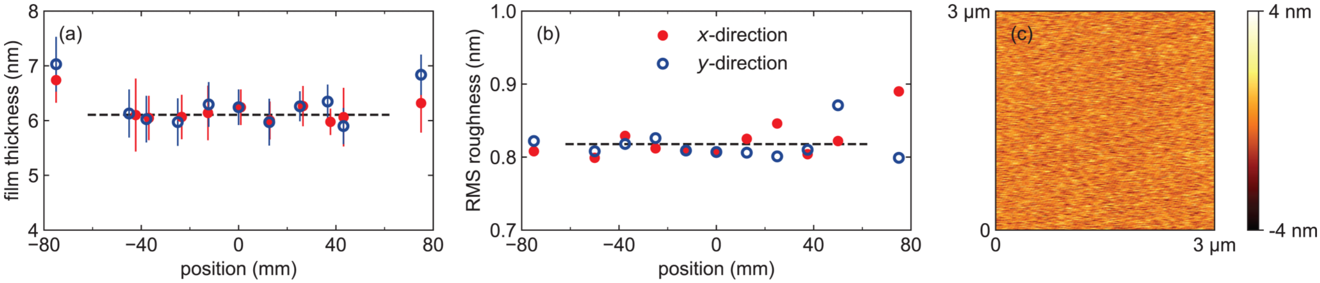

FIG. 1. (a) Spread of film thickness over the position across the wafer table. The error bars correspond to 95% confidence intervals. The horizontal dashed line represents the mean value of 6.1 nm within ± 50 mm from (0, 0). (b) Distribution of root mean square (RMS) surface roughness over a 6-in. area. The horizontal dashed line represents the mean value of 0.82 nm within ± 50 mm. (c) Exemplary $3 \times 3\,\mu m^2$ AFM image at position $y = -37.5$ mm with the mean value as zero level.

chip) distributed along the x- and y-axis of the examined area were characterized. For residual resistivity ρ_0, we took resistance at 25 K and cross sections obtained by a scanning electron microscope (SEM) and AFM measurements. The critical temperature T_c was defined at $0.01\,R_{25}$ and the transition width ΔT as the temperature difference between $0.9\,R_{25}$ and $0.1\,R_{25}$. Current–voltage curves were recorded at 4.2 K to get switching current density j_{sw}. In addition, the temperature dependence of j_{sw} between T_c and 4.2 K was measured on several samples.

III. RESULTS

A. Film thickness and surface roughness

To evaluate geometric film homogeneity, we measured the film thickness and surface roughness within the range of a 6-in. wafer.

Figure 1(a) shows the distribution of film thickness along the x- and y-axis of the examined area. Within a diameter of 4 in. ($|x, y| \leq 50$ mm), there is a negligible variation in thickness around a mean value of 6.1 nm, equivalent to a film inhomogeneity of 3.6%. This corresponds to a growth rate of 0.469 Å/cycle, which is comparable to previously reported values.[25,26] Increasing the area to 6 in. leads to 9.1% inhomogeneity and a maximum thickness of 7.0 ± 0.3 nm ($y = -75$ mm).

The NbN surface roughness is shown in Fig. 1(b), with an exemplary AFM image in Fig. 1(c). The RMS roughness R_q fluctuates around a mean of 0.82 nm, with a maximum of 0.89 nm at $x = +75$ mm. R_q corresponds to roughly two lattice constants of NbN [0.45 nm (Ref. 32)]. A reference measurement of the bare substrate led to similar $R_q = 0.8$ nm. This indicates that ALD-NbN roughness is mainly determined by the surface roughness of the substrate below.

B. Composition and crystal structure

The film composition and crystal properties were determined using XRD and SIMS.

In Fig. 2(a), the normalized intensities of nitrogen and carbon are depicted. It can be seen that the nitrogen concentration slightly varies over an area of 4-in. diameter, whereas there are larger deviations further from the center. The concentration of nitrogen compared to niobium decreases in the range from ± 50 to ± 75 mm in all directions. A similar behavior is observed for carbon. These declining concentrations indicate a niobium-rich composition at the edges of a 6-in. area.

In Fig. 2(b), the diffraction peaks of three samples along the x-axis are given. In the center ($x = 0$ mm), two peaks at 35.49° and 41.34° are detected and can be assigned to the orientations (111) and (200) of δ-NbN, respectively. The full width at half maximum (FWHM) of both peaks is rather large (1.02° and 0.84°), indicating

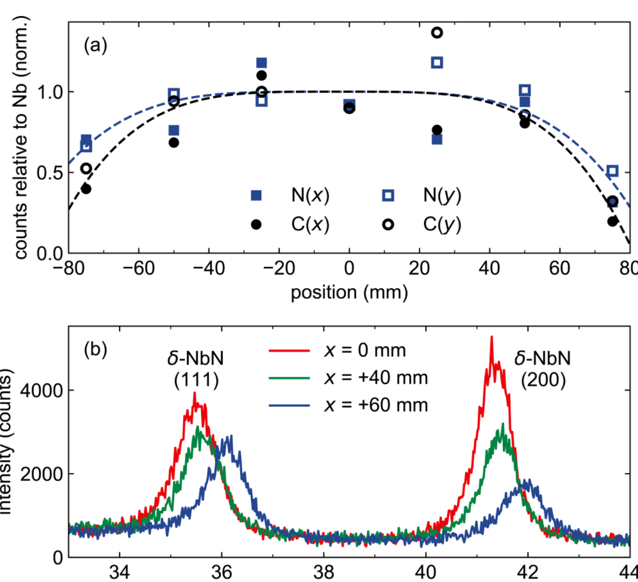

FIG. 2. (a) SIMS: distribution of nitrogen and carbon counts relative to the respective niobium count at each position. Both relative curves are normalized, i.e., the absolute values of nitrogen and carbon cannot be compared. The dashed lines are guides to the eye. (b) XRD: 2Θ-scan (ω fixed at 0.4°) of 20 nm thick ALD-NbN at three positions along the x-axis of the wafer. The two peaks around 35.5° and 41.5° correspond to orientations (111) and (200) of cubic δ-NbN, respectively.

© Author(s) 2021

TABLE I. Peak position, FWHM, and peak area ratio of recorded XRD peaks. For the area ratios of the (111)- to (200)-peaks, we subtracted the baseline of each curve and integrated the peaks in the ranges of (34°–37.5°) and (40°–43°), respectively.

	Peak position (°)		FWHM (°)		Peak area ratio
x (mm)	(111)	(200)	(111)	(200)	(111)/(200)
0	35.49	41.34	1.02	0.84	0.81
40	35.61	41.45	0.98	0.88	1.03
60	36.08	41.91	0.96	1.05	1.57

a nanocrystalline film structure and a distinct lattice parameter spread.[6] Using the Scherrer equation, crystallite sizes of (9–11) nm can be calculated.

At position $x = 40$ mm, the peaks shift to slightly larger angles, but the FWHMs (0.98° and 0.88°) remain nearly constant. Further from the center at $x = 60$ mm, there is a more distinct shift to larger angles, with the peaks at 36.08° (111) and 41.91° (200). Notably, the peak intensity of the (111)-orientation is only slightly dependent on the sample position, while the intensity of (200)-peaks is strongly reduced toward the edge. The disproportionally strong decrease of [100]-crystallites also becomes apparent from the peak area ratios given in Table I.

Within the 2Θ-range (20°–80°), five diffraction peaks from cubic NbN were recorded. Only in the center ($x = 0$ mm), one very small peak from another phase was observed, either from Nb_4N_5 or from niobium oxynitride. Nevertheless, previous investigations revealed the presence of impurities within the deposited films.[6,25] Therefore, the coexistence of amorphous phases of niobium oxides, niobium carbides, and niobium oxynitrides might be possible. The amorphous content, however, should be very small because diffractograms recorded in Bragg–Brentano configuration do not show the occurrence of characteristic "amorphous humps."

C. Superconducting properties

The spread of several superconductivity metrics of the studied NbN film is displayed in Fig. 3. Across a 2-in. diameter, only minimal variation is visible and the electrical parameters approximately amount to $T_c = 10.3$ K, $\Delta T = 1.38$ K, $\rho_0 = 260\,\mu\Omega \cdot$ cm, and $j_{sw} = 5.7$ MA/cm^2. Further distant from the center, the film quality is degrading by varying degree of each property. At $x, y = \pm 50$ mm (corresponding to the edges of a 4-in. wafer), the resistivity is on average increased by 53% compared to the center. Similarly, the switching current density decreases by 45%. The critical temperature is shown to be more stable over the deposition area compared to ρ_0 and j_{sw} and decreases by 10% only. This is expected since T_c is mainly determined by any contiguous, high-quality region along the microbridge. To evaluate film homogeneity, the transition width is better suited because it encompasses the spread of T_c of various regions in the film. From the center to the 4-in. wafer edge, ΔT increases by ~26%. This points to a degrading homogeneity of different grains and regions of the thin film.

Within the uniform area in the center, the critical temperature is in line with what we have previously reported for the same

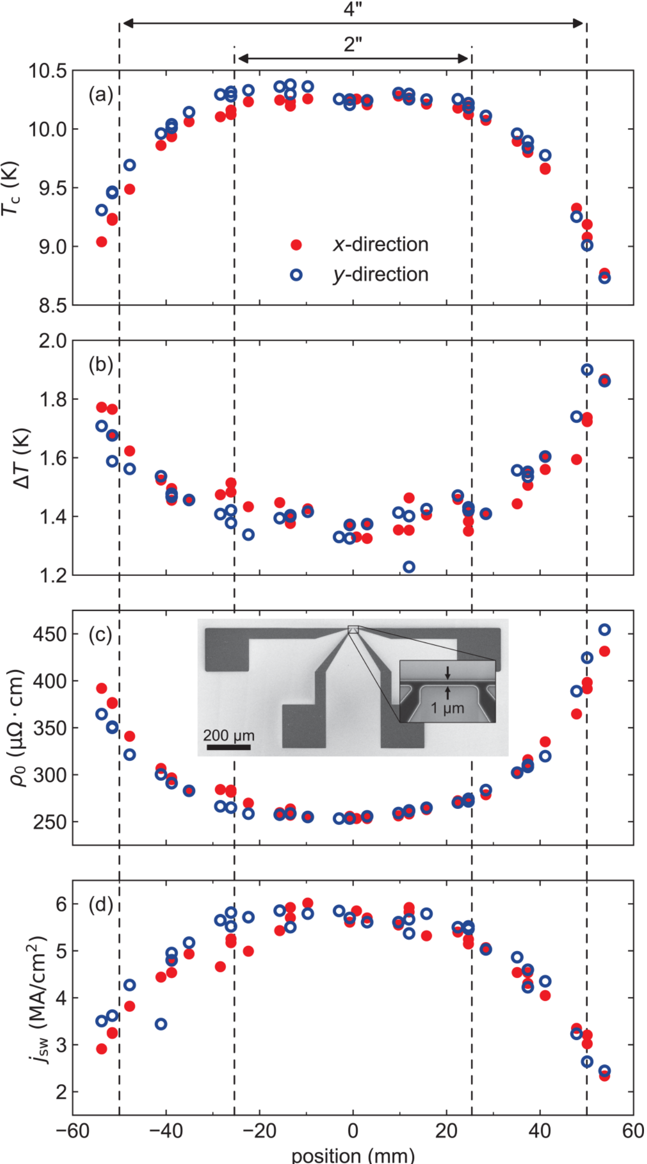

FIG. 3. Distribution of critical temperature (a), superconducting transition width (b), residual resistivity at 25 K (c), and switching current density at 4.2 K (d) over the sample's position on the wafer along the x- and y-axis. The measurements were conducted on microbridges of 1 μm width and 6.1 nm thickness (see the scanning electron micrograph in the inset). The vertical dashed lines illustrate wafer edges of the denoted sizes.

deposition parameters and thickness but on sapphire substrates.[28] From the other metrics, however, ALD-NbN on thermal oxide seems to be a slightly better superconducting material, with a 20% higher j_{sw} and ~20% lower values of ρ_0 and ΔT, respectively. Compared to properties of unpatterned, slightly thicker ALD-NbN on SiN_x reported by Cheng *et al.*,[29] we obtained very similar values

© Author(s) 2021

for ρ_0, while T_c is (2–3) K higher and ΔT about 0.3 K lower in our case. Reasons for this discrepancy could be different deposition temperatures (380 vs 300 °C), plasma gas compositions (pure H_2 vs mixed N_2/H_2), and substrate materials (thermally oxidized Si vs LPCVD-grown SiN_x).

IV. DISCUSSION

We analyzed whether the decreasing j_{sw} toward the wafer edges can be entirely explained by the change of T_c and ρ_0 over the same distance. This can be accomplished by comparing the ratios of the measured switching currents density j_{sw} to the theoretical depairing current density $j_{dep}(0) = 0.74\Delta(0)^{3/2}/(e\rho_0\sqrt{\hbar D})$, with Eq. (31) in Ref. 33, the energy gap $\Delta(0) = 2.05k_B T_c$, the density of states $N(0) = 1/(2e^2\rho_0 D)$, the electron charge e, and the electron diffusion coefficient D.

For the micrometer-wide bridges like in our case, the barrier for vortex entry is considerably reduced compared to (20–100) nm wide bridges.[28,34] This decreases the measurable j_{sw} for $T/T_c \lesssim 0.8$. Although this effect should be similar for all bridges with same dimensions, it introduces an uncertainty because any edge defect can reduce the entry barrier further in a hardly predictable way. This is why we did not take the measured j_{sw}-values at 4.2 K directly but instead recorded $j_{sw}(T)$-curves of each sample and fit the experimental data with

$$j_{fit}(T) = j_{fit}(0) \cdot \left[1 - (T/T_c)^2\right]^{3/2} \tag{1}$$

in the temperature range of $T \geq 0.8T_c$. In this range close to T_c, the coherence length diverges and j_{sw} is mostly determined by the depairing mechanism.[34,35] The fit parameter $j_{fit}(0)$ is then compared to the theoretical value of $j_{dep}(0)$, calculated using the respective T_c and ρ_0 at each x-/y-position. The coefficient D was previously measured to be $0.3\,\mathrm{cm}^2/s$ on comparable ALD-NbN-films of same thickness, albeit on crystalline quartz substrates, and is assumed to be constant over the wafer area.

As shown in Fig. 4(a), the ratio $j_{fit}(0)/j_{dep}(0)$ amounts to $\approx$0.6 in the center. This value is close to what we[28] and others[36] have reported for NbN nanowires at 4.2 K with a width of $\lesssim$200 nm before. Over the examined area, this ratio is almost constant with a maximum deviation of 10% compared to the center. A constant ratio $j_{fit}(0)/j_{dep}(0)$ means that $j_{fit} \propto T_c^{3/2}/\rho_0$ and the measured drop of j_{sw} is in line with the changes in T_c and ρ_0 at each position. The fact that the ratio slightly increases toward the edges is most likely because the assumption of constant diffusion coefficient D is not applicable. Instead, D should decrease toward the edges as it is expected for higher resistivity,[37] and therefore, the ratio $j_{sw,fit}(0)/j_{dep}(0)$ should be lower than calculated.

The degradation in film quality starting at $\sim$25 mm from the center cannot be explained by morphological changes because both the film thickness and surface roughness are fairly uniform within a 4-in. area ($|x, y| \leq 50$ mm). A decreasing nitrogen content in the film relative to niobium was observed, but this could only explain a change of the superconducting properties further distant from the center (> 50 mm).

Instead, XRD measurements suggest changes in the film structure as a possible reason for this drop. The diminishing peak intensity, especially of the (200)-oriented grains, signifies a declining portion of cubic NbN toward the wafer edges. The detected 2Θ-peak shift with increasing distance from the center corresponds to a decrease in the lattice parameter from 4.37 to 4.31 Å. According to the influence of this lattice parameter reduction on the superconducting properties described by Linzen *et al.*,[6] a decrease in T_c by (2–3) K is expected.

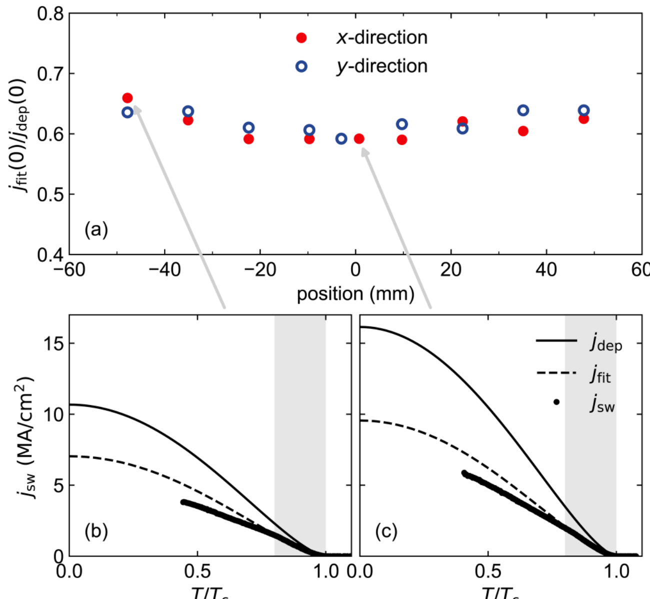

FIG. 4. (a) Distribution of the ratio of fitted current density j_{fit} to theoretical depairing current density j_{dep} at 0 K over the wafer area. (b) and (c) Exemplary $j_{sw}(T)$-curves at $x = -47.8$ mm (b) and $x = 0.7$ mm (c). The dots represent j_{sw} measured on bridges of 1 μm width, the dashed curves denote fits by Eq. (1) to the measured data in the range of $0.8 < T/T_c < 1.0$ (indicated by the shaded area), and the solid line shows the depairing current density j_{dep}, obtained from $j_{dep}(0)$ and temperature dependence in Eq. (1).

The maximum temperature deviation over the substrate table is specified to be ± 2°C. Hence, we do not expect inhomogeneities in deposition temperature to be a factor contributing to film degradation toward the edges.

In previous studies, we found plasma parameters to be crucial for final film composition and electrical properties. A decrease in hydrogen pressure resulted in higher T_c- and j_{sw}-values.[25] In addition, low hydrogen pressure led to an increase in plasma radicals near the substrate surface.[27] This suggests that in the downstream region, the remote plasma could rather act as an active plasma. Moreover, the low pressure additionally prevented interactions of radicals within the downstream due to the increased mean free path, leading to a rather directional plasma exposure. The plasma source in our setup has a diameter of 75 mm and is concentrically aligned above the substrate holder. Therefore, the directional plasma is expected to have its highest energy impact on the substrate within a region of approximately ± 40 mm. This is consistent with our results indicating that the film composition, the lattice

© Author(s) 2021

TABLE II. Summarized parameter spread of ALD-NbN.

		Change (%) over diameter	
Parameter	Center value	2 in.	4 in.
d	6.1 nm	<5	<5
R_q	0.82 nm	<3	<6
T_c	10.3 K	−1	−10
ΔT	1.38 K	+5	+30
ρ_0	260 $\mu\Omega \cdot$ cm	+6	+50
j_{sw}	5.7 MA/cm^2	−8	−45

parameter, and the superconducting properties are significantly altered at distances ≥40 mm from the center in all directions.

Based on these results, the large-area homogeneity of ALD-NbN might be improved by using a larger-diameter plasma source and increasing the ICP–substrate holder distance. This would result in an extended area of uniform plasma distribution and reaction with the deposited precursor.

V. CONCLUSIONS

We have investigated the spread of ALD-NbN film parameters over a 6-in. wafer by studying the morphological, crystalline, and superconducting properties at various positions. All observed film properties including the most decisive switching current density are near-constant over a diameter of 50 mm. Further from the center, at a distance of ±50 mm, we observe larger variations of the electrical properties: +50% (ρ_0), −10% (T_c), +30% (ΔT), and −45% (j_{sw}), while the film thickness and surface roughness are mostly unchanged (see also summary in Table II). XRD measurements suggest that this change of parameters is most likely caused by a shrinking crystalline portion of cubic NbN together with a decrease in the lattice constant.

For the intended purpose of superconducting detectors, these ALD-NbN thin films allow for large-area detector arrays on a 2-in. wafer and could increase the fabrication yield of nanoscale devices compared to conventional reactive magnetron sputtering. The precisely controllable ALD process enables uniform NbN films also of smaller thickness than the investigated 6 nm. Thus, arrangements of a large number of CQPS junction will be feasible on the wafer-scale.

Together with the advantages of precise thickness control, conformal deposition, and moderate deposition temperatures below 400 °C,[38] ALD-NbN thin films are suited for a versatile usage in various further applications, e.g., for back-end-of-line integration with photonic-integrated circuits, for which processing temperatures below (400–500 °C) are necessary.[39,40]

ACKNOWLEDGMENTS

The authors acknowledge the support by Valentin Ripka for film preparation and Uwe Brückner for SIMS measurements. This work was partly supported by the DFG grant (No. SI 704/13-1) and the European Union's Horizon 2020 Research and Innovation Programme under Grant No. 862660/QUANTUM E-LEAPS.

DATA AVAILABILITY

The data that support the findings of this study are available from the corresponding author upon reasonable request.

REFERENCES

[1] A. Shurakov, Y. Lobanov, and G. Goltsman, Supercond. Sci. Technol. **29**, 023001 (2015).
[2] A. A. Adamyan, S. E. Kubatkin, and A. V. Danilov, Appl. Phys. Lett. **108**, 172601 (2016).
[3] J. Luomahaara, V. Vesterinen, L. Grönberg, and J. Hassel, Nat. Commun. **5**, 4872 (2014).
[4] S. E. de Graaf *et al.*, Nat. Phys. **14**, 590 (2018).
[5] J. T. Peltonen *et al.*, Phys. Rev. B **88**, 220506 (2013).
[6] S. Linzen, M. Ziegler, O. V. Astafiev, M. Schmelz, U. Hübner, M. Diegel, E. Il'ichev, and H.-G. Meyer, Supercond. Sci. Technol. **30**, 035010 (2017).
[7] F. Marsili *et al.*, Nat. Photonics **7**, 210 (2013).
[8] B. Korzh *et al.*, Nat. Photonics **14**, 250 (2020).
[9] Y. Hochberg, I. Charaev, S.-W. Nam, V. Verma, M. Colangelo, and K. K. Berggren, Phys. Rev. Lett. **123**, 151802 (2019).
[10] H. Zhou, Y. He, L. You, S. Chen, W. Zhang, J. Wu, Z. Wang, and X. Xie, Opt. Express **23**, 14603 (2015).
[11] L. Chen, D. Schwarzer, J. A. Lau, V. B. Verma, M. J. Stevens, F. Marsili, R. P. Mirin, S. W. Nam, and A. M. Wodtke, Opt. Express **26**, 14859 (2018).
[12] J. P. Allmaras, E. E. Wollman, A. D. Beyer, R. M. Briggs, B. A. Korzh, B. Bumble, and M. D. Shaw, Nano Lett. **20**, 2163 (2020).
[13] E. E. Wollman, V. B. Verma, A. E. Lita, W. H. Farr, M. D. Shaw, R. P. Mirin, and S. W. Nam, Opt. Express **27**, 35279 (2019).
[14] S. Miyajima, M. Yabuno, S. Miki, T. Yamashita, and H. Terai, Opt. Express **26**, 29045 (2018).
[15] Q.-Y. Zhao, D. Zhu, N. Calandri, A. E. Dane, A. N. McCaughan, F. Bellei, H.-Z. Wang, D. F. Santavicca, and K. K. Berggren, Nat. Photonics **11**, 247 (2017).
[16] S. Doerner, A. Kuzmin, S. Wuensch, I. Charaev, F. Boes, T. Zwick, and M. Siegel, Appl. Phys. Lett. **111**, 032603 (2017).
[17] B. Baek, A. E. Lita, V. Verma, and S. W. Nam, Appl. Phys. Lett. **98**, 251105 (2011).
[18] V. B. Verma *et al.*, Opt. Express **23**, 33792 (2015).
[19] I. Charaev, Y. Morimoto, A. Dane, A. Agarwal, M. Colangelo, and K. K. Berggren, Appl. Phys. Lett. **116**, 242603 (2020).
[20] A. Semenov *et al.*, Phys. Rev. B **80**, 054510 (2009).
[21] S. Miki, T. Yamashita, H. Terai, and Z. Wang, Opt. Express **21**, 10208 (2013).
[22] A. Engel, A. Aeschbacher, K. Inderbitzin, A. Schilling, K. Il'in, M. Hofherr, M. Siegel, A. Semenov, and H.-W. Hübers, Appl. Phys. Lett. **100**, 062601 (2012).
[23] A. Vetter *et al.*, Nano Lett. **16**, 7085 (2016).
[24] A. E. Dane, A. N. McCaughan, D. Zhu, Q. Zhao, C.-S. Kim, N. Calandri, A. Agarwal, F. Bellei, and K. K. Berggren, Appl. Phys. Lett. **111**, 122601 (2017).
[25] M. Ziegler *et al.*, IEEE Trans. Appl. Supercond. **27**, 1 (2017).
[26] M. J. Sowa, Y. Yemane, J. Zhang, J. C. Palmstrom, L. Ju, N. C. Strandwitz, F. B. Prinz, and J. Provine, J. Vac. Sci. Technol. A **35**, 01B143 (2017).
[27] M. Ziegler, L. Fritzsch, J. Day, S. Linzen, S. Anders, J. Toussaint, and H.-G. Meyer, Supercond. Sci. Technol. **26**, 025008 (2013).
[28] E. Knehr, A. Kuzmin, D. Y. Vodolazov, M. Ziegler, S. Doerner, K. Ilin, M. Siegel, R. Stolz, and H. Schmidt, Supercond. Sci. Technol. **32**, 125007 (2019).
[29] R. Cheng, S. Wang, and H. X. Tang, Appl. Phys. Lett. **115**, 241101 (2019).
[30] G. G. Taylor, D. V. Morozov, C. T. Lennon, P. S. Barry, C. Sheagren, and R. H. Hadfield, Appl. Phys. Lett. **118**, 191106 (2021).
[31] J. R. Clem and K. K. Berggren, Phys. Rev. B **84**, 174510 (2011).
[32] Z. Wang, A. Kawakami, Y. Uzawa, and B. Komiyama, J. Appl. Phys. **79**, 7837 (1996).
[33] J. R. Clem and V. G. Kogan, Phys. Rev. B **86**, 174521 (2012).

© Author(s) 2021

[34]K. Il'in, M. Siegel, A. Engel, H. Bartolf, A. Schilling, A. Semenov, and H.-W. Huebers, J. Low Temp. Phys. **151**, 585 (2008).
[35]K. K. Likharev, Rev. Mod. Phys. **51**, 101 (1979).
[36]S. Frasca *et al.*, Phys. Rev. B **100**, 054520 (2019).
[37]D. Henrich, S. Dörner, M. Hofherr, K. Il'in, A. Semenov, E. Heintze, M. Scheffler, M. Dressel, and M. Siegel, J. Appl. Phys. **112**, 074511 (2012).
[38]For plasma ALD, lower deposition temperatures are possible than for thermal ALD. Nevertheless, depositing nitrides at lower temperatures is challenging because of oxidation and carbon impurities.[41] From previous measurements on ALD-NbN films,[26,27] a lower deposition temperature goes along with a higher resistivity, lower critical temperature, lower film density, and smaller crystallite sizes. Reducing the temperature from 400 to 300 °C led to 2 K lower T_c.[27] At 150 °C, T_c of 22 nm thick films was found to be ∼6 K.[26]
[39]Y. H. D. Lee and M. Lipson, IEEE J. Sel. Top. Quantum Electron. **19**, 8200207 (2013).
[40]M. Schwartz *et al.*, Nano Lett. **18**, 6892 (2018).
[41]H. C. M. Knoops, T. Faraz, K. Arts, and W. M. M. E. Kessels, J. Vac. Sci. Technol. A **37**, 030902 (2019).

© Author(s) 2021